

DEEP PERONA–MALIK DIFFUSIVE MEAN SHIFT IMAGE CLASSIFICATION FOR EARLY GLAUCOMA AND STARGARDT DISEASE DETECTION

Senthil kumar.Arunachalam^{1}, Somasundaram. Devaraj², Bhavani Sridharan³*

^{1,3}Department of Electronics and Communication Engineering, Sri Shakthi Institute of Engineering and Technology, Coimbatore-641062, Tamilnadu, India

²School of Electronics Engineering, Vellore Institute of Technology, vellore-632014, Tamilnadu, India

Email: doubleinstru@gmail.com^{1*}(corresponding author), somgce@gmail.com², bhavanisridharan7@gmail.com³

DOI: <https://doi.org/10.22452/mjcs.vol36no1.2>

ABSTRACT

Glaucoma and Stargardt's, an inherited disease predominantly affect the retinal portion of the eye. The diagnosis of Glaucoma in a fundus image is an arduous, time consuming process. There were many research works carried out to detect early stages of Glaucoma and Stargardt's disease. However, the accuracy, diagnostic time and performance were not improved. To resolve the above said problems, a computational method called Deep Neural Perona–Malik Diffusive Mean Shift Mode Seeking Segmented Image Classification (DNP-MDMSMSIC) is introduced for the early detection of Glaucoma and Stargardt's disease with retinal fundus images. The DNP-MDMSMSIC method comprises diverse types of layers that support to identify early detection of disease with improved accuracy and less time. Process as explained; initially, numerous qualified retinal images are given as input to the input layer. These input images are transmitted further to the hidden layer 1 to perform image pre-processing. In DNP-MDMSMSIC, Space-Variant Perona–Malik Diffusive Image Preprocessing is carried out to decrease the noise from input image without removing contents like edges, lines, etc., for image interpretation with a higher peak signal-to-noise ratio. This preprocessed image is further processed in the hidden layer 2 where the feature extraction process is performed to extract features like color, texture, and intensity with a higher degree of accuracy. Based on the extracted features, an input feature image gets segmented in hidden layer 3. Mean Shift Mode Seeking Segmentation algorithm is employed to segment the pixels in image space with corresponding feature space points. Then the segmented images are given to the output layer to perform retinal fundus image classification using Bregman Divergence Function. During the image classification, the distance between two segmented regions (i.e., testing image region of particular class and training image region) with convex is measured. In this way, the retinal fundus images get classified with higher accuracy. Experimental evaluation is performed by considering the metrics such as peak signal-to-noise, disease detection accuracy, disease detection time, and error rate corresponding to the number of retina fundus images and image size. DNP-MDMSMSIC method is designed to detect Glaucoma and Stargardt's disease at an earlier stage with higher accuracy by 8% and less time by 20% with aid of ACRIMA database.

Keywords: *Glaucoma detection, Stargardt's disease, retinal fundus image, Space-variant Perona–Malik diffusive, Feature extraction, Mean shift mode seeking, pixel segmentation, Bregman divergence function, Classification.*

1.0 INTRODUCTION

Glaucoma and Stargardt's disease are considered as one of critical eye diseases which could lead to complete blindness. Glaucoma and Stargardt's disease are estimated to affect 79.6 million people by 2020. No symptoms reflected in early stages, however gradually over the period of time affect the irreversible vision loss by damaging the optic nerve. Glaucoma, chronic eye disease affects the optic nerve and neural fiber bundle. The optic nerve performs the function of visual information transfer from the eye to the brain. [8]. Glaucoma symptoms are severe eye pain, nausea, vomiting, redness in your eye, sudden vision disturbances, seeing colored rings around lights, and sudden blurred vision.

Glaucoma is a progressive eye disease due to the increase in intraocular pressure. Accurate early detection may prevent vision loss [8]. Stargardt's disease is a general kind of hereditary macular dystrophy in the child and is one of the most genetic disorders which cause macular degeneration. Stargardt's disease is variable and provides low loss of central vision

in both eyes. The disease causes progressive damage or degeneration of the macula, which is tiny area in the center of the retina, responsible for clear, sharp and Straight-ahead vision [24]. The detection of these diseases at an earlier stage is mandatory for preventing blindness. The earlier identification of glaucoma saves the patient from blindness. Segmentation and classification methods are important to determine the eye disease at a prior stage [8].

The eye diseases such as Glaucoma and Stargardt's disease are used to visualize optic disc, retina, and blood vessels. In addition, retinal blood vessel pattern is inimitable for humans. It is a very stable pattern in biometric determination. The optic disc is the initial stage of the optic nerve and is caused by damage to thin blood vessels. The narrowed blood vessel minimizes the circulation of blood to the connected body element. The tiny blood vessels in the back of the eye are deteriorated and leak fluid into and under the retina. This causes the retina to enlarge leads to blurring or distorting of vision, abnormal capabilities causes breakage and leads to bleeding. So, the novel deep learning classification method is used to improve the time complexity and accuracy for automatically detecting Glaucoma and Stargardt's disease in the early stage. The example of normal fundus image and fundus images with Glaucoma and Stargardt's disease is collected from the ACRIMA database, retina image bank database is shown in figure 1.

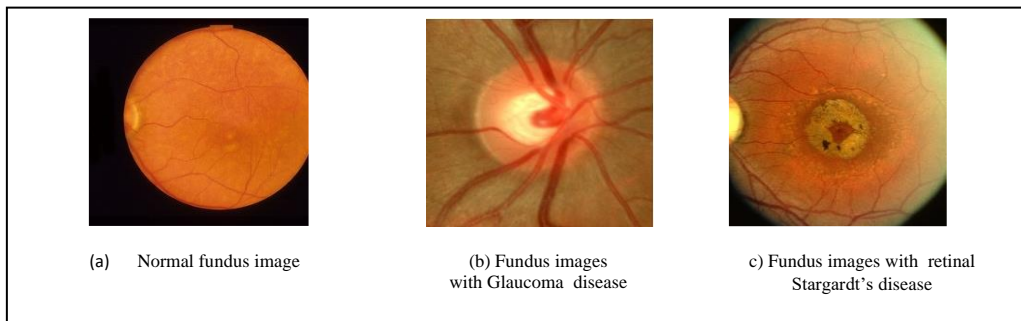


Fig. 1: Example of normal fundus image and fundus images with Glaucoma and Stargardt's disease

1.1 Problem statement

The early stage of glaucoma identification is a vital role to avoid blindness. Several techniques have been developed to discover eye disorders through fundus images in a precise manner. However, the quality of input images was not enhanced. Traditional image filtering concepts are employed for enhancing the image. However, PSNR was not adequately enhanced. In addition, classification approaches were developed with higher accuracy. However, the time consumed to determine illness was not minimized without compromising accuracy. Then, feature extraction and segmentation processes were performed before classifying the images, hence failed to extract the robust features for disease prediction. In order to solve this issue, novel techniques are needed for early disease detection.

The major contributions of the DNP-MDMSMSIC method are summarized as follows,

- ❖ To increase peak signal-to-noise ratio as compared to existing works, Space-Variant Perona–Malik Diffusive Image Pre-processing is introduced in the DNP-MDMSMSIC method. It determines the difference between two neighboring pixels and eliminates the noisy pixels with strong diffusion action.
- ❖ To minimize the disease detection time, the feature extraction process is used to deeply extract the features (i.e., color, texture, and intensity) with aid of a deep neural network. After the feature extraction, the Mean Shift Mode Seeking Segmentation algorithm is employed to partition the image pixels. By estimating the similar neighboring pixels, the Gaussian kernel is used via distance measure. The mean shift procedure for detecting local maxima of modes to segment the images. In this way, the similar pixels in the image are segmented with minimum time.
- ❖ To increase the disease detection accuracy with less error rate, Bregman Divergence Function is employed in the DNP-MDMSMSIC method where it measures the distance between the testing image region of a certain class and the training image region through the convex function. When the distance between the testing image and training image is minimum, then the retinal fundus image is categorized as an abnormal image (i.e., Glaucoma, Stargardt's disease). When the distance between two images is maximum, then the image is categorized as a normal image. This helps to categorize the retinal fundus images into different classes for detecting the disease.

The organization of the paper is described as follows. Section 2 discusses the literature review with its advantages and shortcomings. Section 3 provides the proposed methodology with an architecture diagram. Experimental settings are provided in section 4 which gives the details about the implementation of the method. The results and discussion is done in Section 5 which includes a description of evaluation measures and performance analysis. The conclusion is drawn towards the end of the paper in Section 6.

2.0 RELATED WORKS

Optic Disc (OD) localization method was implemented in [1] to recognize the different diseases through the retinal images. The designed method comprises three processes such as circle distribution, circle detection, and circle center distribution. But, the error during the disease detection was not minimized. Deep convolution neural network (DCNN) was designed in [2] to discover the abnormality in retinal fundus images for improving the accuracy. The disease detection time was not reduced by using DCNN. Regional classification framework was introduced in [3] for accurate localization and segmentation of optic disc, But, the error rate was not focused. In [4], bit-plane and local binary pattern-based technique was designed for glaucoma recognition. Decision level-based fusion technique was used for enhancing the overall performance. The designed method does not use pre-processing method since the noise ratio was not minimized.

Deep learning-based glaucoma classification network (GC-NET) was designed in [5] to identify the glaucoma diseases by means of categorizing the retinal images. But, the time to classify the disease was not effectively reduced. Gradient-Boosting Classifier was designed in [6] to categorize moderate glaucoma at an earlier stage. The designed classifier integrates vessel density and tissue thickness determination for glaucoma detection. However, the time taken to classify glaucoma was more. A novel algorithm for automatic optic disc segmentation on fundus images were presented in [7] depended on the Circular Hough Transform (CHT), Polar Transform, and B-spline approximation. However, the peak signal-to-noise ratio was not analyzed by using the pre-processing algorithm. Optic Cup segmentation was implemented in [8] by using glowworm swarm optimization to discover glaucoma. Though accuracy was improved, the error rate was minimized. Glaucoma screening and recognition were performed in [9] based on the fully automated scheme. Cup-to-Disc Ratio features are taken to discover the occurrence of glaucoma from retinal fundus images. However, the computation time was not reduced effectively. A deep learning technique was designed in [10] to execute glaucoma detection. But the accuracy was not enhanced sufficiently by using the deep learning technique.

A glaucoma detection algorithm was developed in [11] for distinguishing the normal and abnormal images. But the designed algorithm uses more time while analyze texture features. According to the machine learning algorithms, a novel system was introduced in [12] to discover glaucoma. However, the noise reduction was not performed with the pre-processing method. Two-layer sparse auto encoder was presented in [13] to perform accurate recognition of glaucoma from retinal fundus images. However, the performance of detection was not enough when considering a large number of images. Two-stage solution for optic disc localization and classification was designed in [14] for glaucoma detection. But more effort is required to detect glaucoma with reliability.

A review of segmentation and classification approaches was analyzed in [15] for glaucoma diagnosis. Though, the noise elimination was not focused. Through the region-based pixel density calculation method, an improved image processing model was employed in [16] to partition the optic disc. However, the performance of feature extraction was not sufficient. Multi structure descriptor was designed in [17] for diagnosing glaucoma at an early stage. Hybrid neural network classifiers were employed to categorize the healthy and glaucomatous images. But the classification accuracy was effectively improved. An automated approach to detect glaucoma was presented in [18] through the texture and CNN descriptors. But accuracy was not increased with less time.

An automatic detection scheme was introduced in [19] for diagnosing glaucoma. But the error rate was not reduced during the classification. Multi-Feature Vector and Deep Belief Network (MFV-DBN) was developed in [20] to determine glaucoma at an earlier stage. Though the method increases the accuracy, the time complexity was not effectively decreased. An automated detection system was introduced in [21] for screening of diabetic retinopathy. However, the accuracy was not increased. A convolution neural network was introduced in [22] to segment the optic disc, fovea, and blood vessels. An automated system was introduced in [23] for EXs detection and classification in fundus images. However, the accuracy was not increased. But, it failed to reduce the noise ratio.

Classification of glaucoma network (CoG-NET) was introduced in [25] to discover the glaucoma disease. But, the early detection of glaucoma disease was not considered. A new optic disc and optic cup segmentation method were developed

in [26] for obtaining the glaucoma disease. Contextual information enhanced convolutional neural networks were designed in [27] to correctly detect the retinal vessel segmentation. However, the time was higher. Support Vector Machine (SVM) was introduced in [29] for binary classification. The designed machine failed to remove the noise.

3.0 DNP-MDMSMSIC METHOD

DNP-MDMSMSIC method is introduced to perform Glaucoma and Stargardt’s detection and classification by four different processes such as pre-processing, feature extraction, segmentation, and classification. A number of Retinal fundus images as input taken from ACRIMA database, retina image bank database, and DIARETDB0 - Standard Diabetic Retinopathy Database. In this work, preprocessing model uses Space-Variant Perona–Malik Diffusion to minimize the noise in the retinal fundus image for improving the image quality. On the contrary to the existing algorithm, feature extraction applies a deep neural network to learn the features for automatically extracting color, texture, and intensity features with lesser time. Followed by, Image segmentation utilizes a mean shift mode seeking segmentation algorithm to separate the similar pixels in the image. The Bergman divergence function is used to measure the distance between the testing image and the testing image via convex function. This assists to classify the retinal fundus images into dissimilar classes for identifying the disease. Therefore, the proposed DNP-MDMSMSIC method is suitable for Glaucoma and Stargardt’s Disease identification. DNP-MDMSMSIC Method is introduced for the detection of Glaucoma and Stargardt’s Disease shown in figure 2.

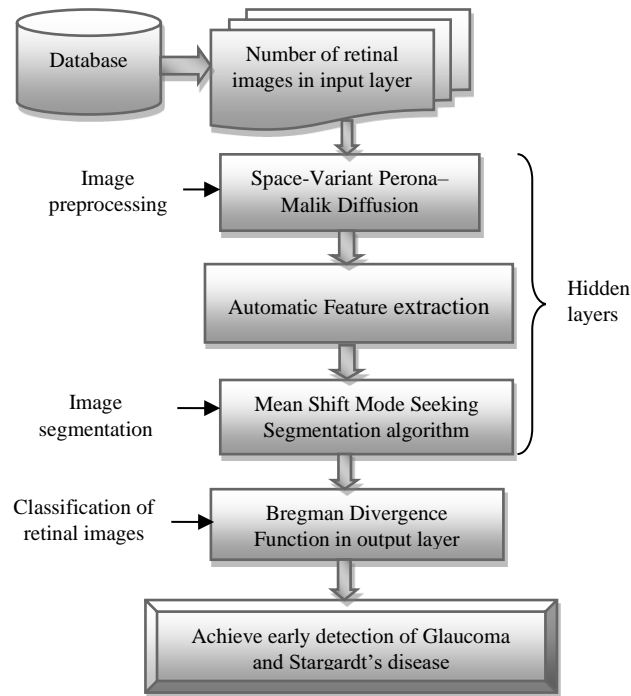


Fig. 2: DNP-MDMSMSIC Method for Early Glaucoma and Stargardt’s Disease Detection

In this method, Glaucoma and Stargardt’s detection and classification are carried out with different processes. In the deep learning network, nervous system cells are termed neurons. Neurons are the cells that send, receive, and transmit chemical and electrical signals in the brain. Number of Retinal fundus images is taken from ACRIMA database. At first, the retinal fundus image is used as input. These input images are fed into hidden layer one for pre-processing. In the deep neural network, the first layer is represented as the input layer, and the last layer is denoted as the output layer. One or more intermediate layers are hidden. These intermediate layers are called hidden layers for the reason that they are not straightly observable from inputs and outputs. The pre-processed image results are given to hidden layer two where the feature extraction process is carried out to obtain the features like color, texture, and intensity. After that, mean shift mode seeking segmentation is applied for segmenting pixels in image space. The segmented images are classified into normal, and abnormal. This aids to enhance the accuracy of glaucoma and Stargardt’s disease.

Consider the number of retinal fundus images ' $I = I_1, I_2, I_3, \dots, I_n$ ' where ' n ' denotes, the total number of images in ACRIMA database ' D '. The neuron process in input layer ' u ' is given by,

$$u(t) = \sum_{i=1}^n I_i \varepsilon_{uv} + b_j \quad (1)$$

From (1), ' $u(t)$ ' represents the process of neurons in the input layer at time ' t ', ' ε_{uv} ' represents weight between input and hidden layer and ' b_j ' is a biased term.

3.1 Space-Variant Perona–Malik Diffusive Image Pre-processing

In image processing, pre-processing is a mandatory step to remove the noise comprised in the input image. In the DNP-MDMSMSIC method, the retinal input fundus images from the input layer are submitted to preprocessing process in which the noise presented input image is eliminated. This is performed with the aid of Space-Variant Perona–Malik Diffusion. Anisotropic diffusion commonly called Perona–Malik diffusion was introduced by Perona and Malik in 1987 to reduce image noise and preserve the edges. Anisotropic diffusion is a non-linear and space-variant transformation of the original image. Space-Variant Perona–Malik Diffusion is a preprocessing model to minimize the noise in the retinal fundus image. The process of space-variant Perona–Malik diffusive image pre-processing is illustrated as follows.

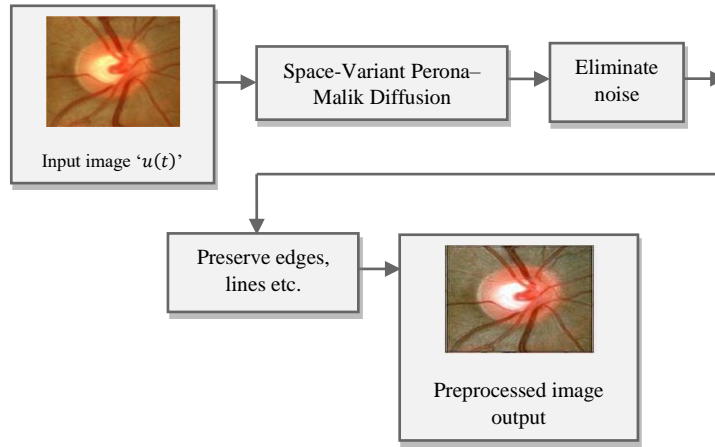


Fig. 3: Space-Variant Perona–Malik Diffusion Image Pre-processing

Figure 3 demonstrates the process of image pre-processing using space-variant Perona–Malik diffusion for increasing the peak-signal to noise ratio. During this process, a significant part of the image content such as edges, and lines is not affected for further image analysis. In DNP-MDMSMSIC method, pre-processing is performed in hidden layer 1. Figure 3 shows Space-variant Perona–Malik diffusion and its equation is expressed as,

$$\frac{\partial I(u,v,t)}{\partial t} = \text{div}[C(\|\nabla I(u,v,t)\|)\nabla I(u,v,t)] \quad (2)$$

From (2), ' $I(u,v,t)$ ' denotes input retinal fundus image, ' $\nabla I(u,v,t)$ ' denotes gradient version of an image to preserve edges, ' t ' refers to the time parameter, the gradient magnitude is introduced by ' $(\|\nabla I(u,v,t)\|)$ ', c is known as the conductance function, that reducing feature of the gradient magnitude. By using this function, it is employed to assure limit $x \rightarrow 0$ $c(u) = 1$, so that the diffusion is maximal within uniform regions, and limit $x \rightarrow \infty$ $c(u) = 0$, so that the diffusion is stopped across edges. The conductance function that manages diffusion strength, and ' div ' is a divergence operator. The diffusion strength is simulated with a gradient of input image intensity. Anisotropic diffusion maintains image structure, textures, and edges. Perona and Malik discretized the above diffusion expression and obtained as,

$$I_m^{t+1} = I_m^t + \sum_{n \in \eta_m} C(|\nabla I_{m,n}|)\nabla I_{m,n} \quad (3)$$

From (3), ' I_m^t ' refers intensity of pixel 'm' from image I at instant 't', ' η_m ' refers spatial neighborhoods (i.e., North, South, East and West neighbors) of current pixel 'm', ' C ' is conductance function. Then the difference between neighboring pixels in each direction is expressed as,

$$\nabla I_{m,n} = I_n^t - I_m^t \text{ Where } n \in \{N, S, E, W\} \quad (4)$$

From (4), ' I_m^t ' denotes intensity of current pixel 'm' and ' I_n^t ' denotes intensity of neighboring pixel 'n'. Substitute equation (4) in (3), then obtained as,

$$I_m^{t+1} = I_m^t + \sum_{n \in \{N, S, E, W\}} C(I_n^t - I_m^t) \cdot (I_n^t - I_m^t) \quad (5)$$

From (5), the noise pixel provides strong diffusion action and image contrast is improved. In proposed DNP-MDMSMIC method, the deep neural network automatically learns features for extracting the color, texture, and intensity features from input preprocessed images in the hidden layer. This aids to decrease the disease detection time as shown in figure 4. With the extracted features, these images are segmented.

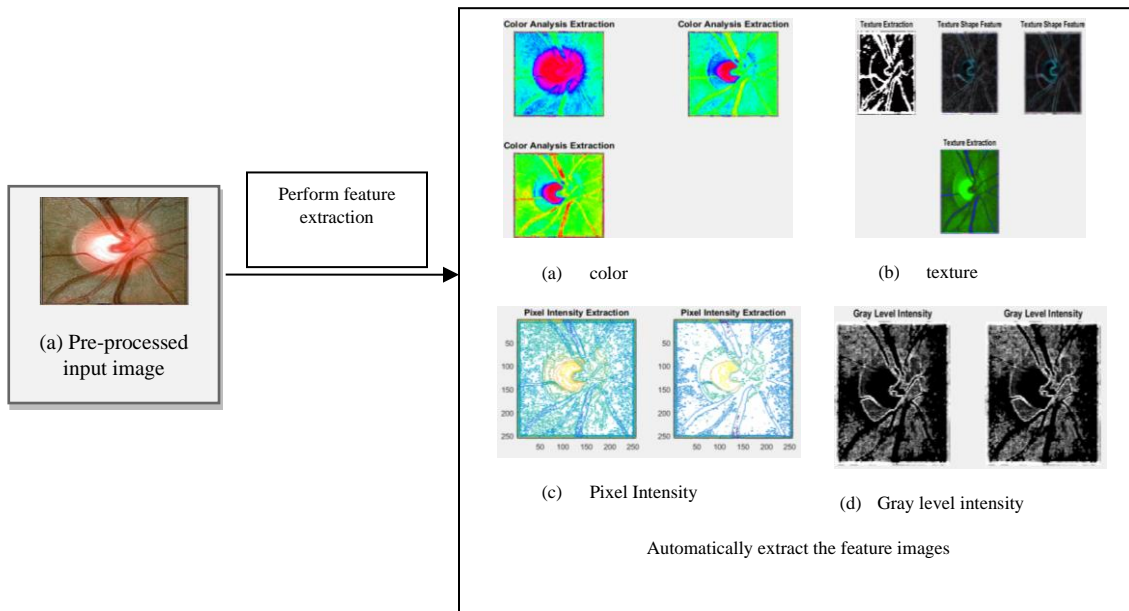


Fig. 4: Feature extraction (a) Pre-processed input image (b) Automatically extract the feature images

3.2 Mean Shift Mode Seeking Segmentation Algorithm

In the third hidden layer, the segmentation process is performed. Mean shift is a non-parametric iterative model-based algorithm for locating the maxima modes for each pixel so-called mode-seeking algorithm was developed by Fukunaga and Hostetler in 1975. The mean shift mode-seeking segmentation algorithm shown in figure 5 is a non-parametric iterative mode-based algorithm. It is employed to determine the maximum density function. Mean Shift Mode Seeking algorithm is an efficient method to detect the mode of each pixel for segmentation.

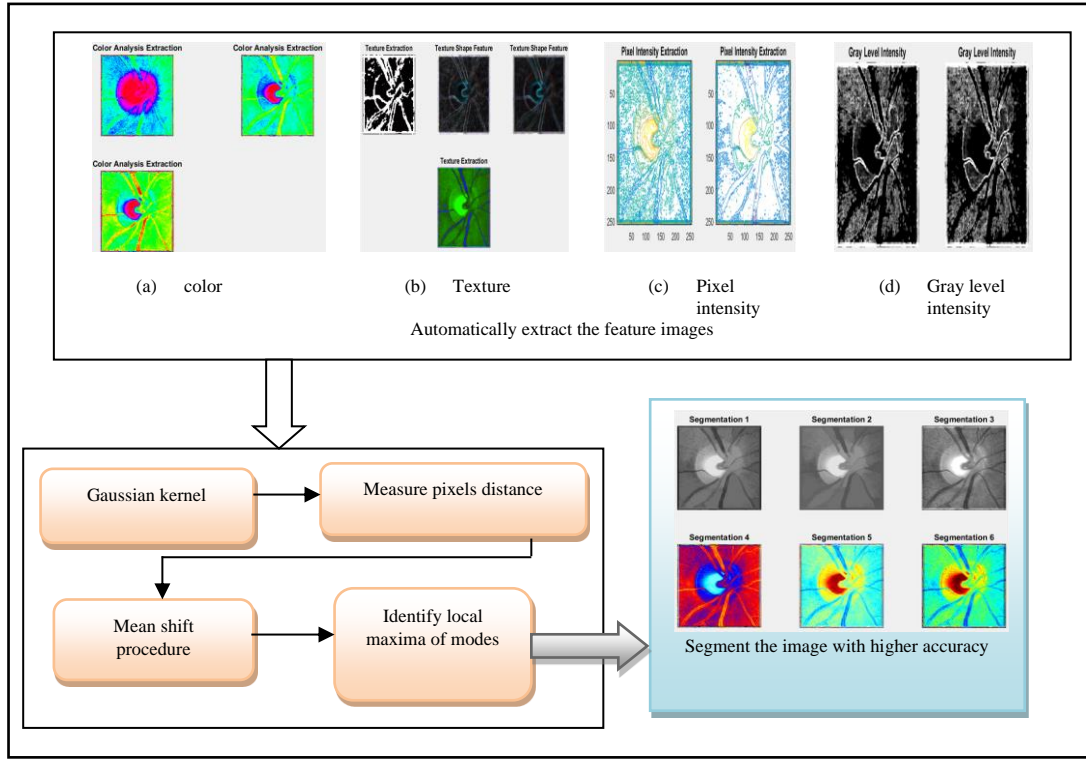


Fig. 5: Mean Shift Mode Seeking Segmentation Algorithm

Mean Shift Mode Seeking algorithm detects the mode of each pixel for segmentation. The mean shift mode seeking segmentation algorithm partitions the pixels with feature space points. The segmentation algorithm uses a Gaussian kernel to determine similar neighboring pixels via distance measure. The Gaussian kernel is optimal since it includes a smooth trajectory for convergence. Then the mean shift procedure is employed for segmenting images by detecting local maxima modes for each pixel. With this, the more similar pixels are segmented with higher accuracy.

Consider the number of pixels in the input feature extraction image. The Gaussian kernel function identifies the distance between two pixels and is expressed as,

$$G(I_m, I_n) = \frac{1}{2\sigma^2} \exp^{-\left(\frac{\|I_n - I_m\|^2}{2\sigma^2}\right)} \quad (6)$$

From (6), ‘ G ’ represents a Gaussian kernel function, ‘ $\|I_n - I_m\|^2$ ’ indicates a squared distance between a neighboring pixel of image ‘ I_n ’ and current pixel of image ‘ I_m ’ and ‘ σ ’ denotes a deviation. The minimal distance among pixels is considered for segmenting process. After computing the distance between each pixel, the mean shift procedure is carried out to segment similar pixels in the image. Then the mean shift based on the Gaussian kernel is given by,

$$M(I_m) = \frac{\sum_{n=1}^N G(I_n - I_m) \cdot I_n}{\sum_{n=1}^N G(I_n - I_m)} \quad (7)$$

From (7), $M(I_m)$ refers to a mean shift. ‘ $M(I_m)$ ’ is determined for each pixel in the image. This process is repeated until attaining convergence. The pre-processed image is segmented in hidden layer three. Thus, the process of neurons in the hidden layers is obtained as follows,

$$v_i(t) = M(I_m) \sum_{i=1}^n u(t) \varepsilon_{v_i} \quad (8)$$

From (8), ‘ $v_i(t)$ ’ denotes the process of neurons in hidden layers at a time ‘ t ’ and ‘ ε_{v_i} ’ denotes the weight of hidden layers. From the above expression, the retinal images are segmented. The results of segmented images are given to the output layer where the classification is performed to identify the disease.

3.3 Bregman Divergence Function

Bregman divergence is a measure of the difference between two points via convex function was presented by Lev M. Bregman in 1967. The Bergman divergence function is applied at the output layer in the DNP-MDMSMSIC method for classifying the segment for identifying disease at an early stage. In the DNP-MDMSMSIC method, Bregman Divergence Function computes the distance between two segmented regions (i.e., testing image region of a particular class and training image region) through convex function.

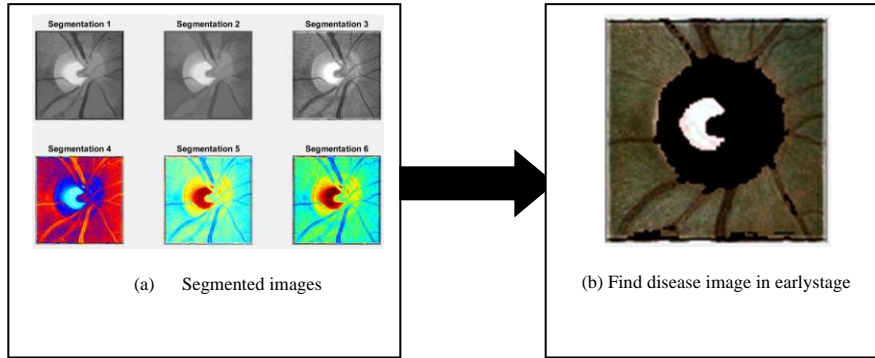


Fig. 6: Bergman divergence function (a) segmented input image (b) Find disease image in early stage

Figure 6 shows the Bergman divergence function of input and output images. Thus, the Bergman divergence function is measured as [28],

$$B_F(x_I, y_I) = F(x_I) - F(y_I) - \langle \nabla F(y_I), x_I - y_I \rangle \quad (9)$$

From (9), ' B_F ' denotes the Bergman divergence function, ' x_I ' denotes the testing image and ' y_I ' indicates a training image. If the distance between the testing image and the training image is less, then the retinal fundus image is classified as an abnormal or diseased image. Or else, it is classified as normal. The neuron process in the output layer is given by,

$$w(t) = B_F(x_I, y_I)(v_i(t)\varepsilon_{vw}) \quad (10)$$

From (10), ' $w(t)$ ' denotes activity of neuron at time ' t ' and ' ε_{vw} ' denotes weight between hidden and output layer. Where $E(t)$ expressed by,

$$E(t) = w(t)' - w(t) \quad (11)$$

From (11), ' $E(t)$ ' denotes the error rate, ' $w(t)'$ ' denotes predicted output and ' $w(t)$ ' refers to actual output. Based on the error rate, weights are updated and determine minimal error output for disease detection. From that, glaucoma and Stargardt's disease detection is performed in the DNP-MDMSMSIC method with higher accuracy and less time.

4.0 EXPERIMENTAL SETTINGS

The performance of the DNP-MDMSMSIC method, existing [1], [2] and [29] are implemented in MATLAB with ACRIMA database, retina image bank database, and DIARETDB0 - Standard Diabetic Retinopathy Database. Based on the objective of the proposed method (i.e., focused on accuracy with lesser disease detection error, and disease detection time) the existing methods such as OD localization and DCNN are taken as base paper. These two existing methods are recent and relevant papers in the proposed method. Existing OD localization was employed to detect disc candidate locations. However, the disease detection error was not minimized. Existing DCNN was utilized for finding the abnormality in retinal fundus images. But, it failed to lessen the disease detection time. By considering the above two problems of these methods, the proposed DNP-MDMSMSIC method concept is derived. The drawbacks of these methods are effectively convinced by implementing the proposed DNP-MDMSMSIC method.

In order to conduct the experiment, The MATLAB 2015 b platform is used to develop the proposed method, the different toolboxes are used for software and hardware requirements such as Windows 10 Operating system, core i3-4130 3.40GHZ

Processor, 4GB RAM, 1TB (1000 GB) Hard disk, ASUSTek P5G41C-M Motherboard, Internet Protocol. The ACRIMA database [30], retina image bank database [31], and DIARETDB0 - Standard Diabetic Retinopathy Database [32] are divided into two sets such as training and validation. 70% of images are employed for training and the remaining 30% of images are applied for validation for each dataset. The runtime is measured as the amount of time taken by the algorithm to run based on CPU execution time, processor speed, instruction set, disk speed, and brand of the compiler. The overall proposed DNP-MDMSMSIC method run time is 27ms for conducting the experiments.

Table 1: Three dataset information

ACRIMA database	Year	2019
	Dataset size	25MB
	Total image	705
	Retinal fundus images are categorized as glaucomatous or abnormal	396
	Normal images	309
	Retinal fundus image size (KB)	21.3, 15.4, 9.13, 16.5, 19.7, 26.3, 17.9, 32.2, 11.7, 10.2
	No. of Retinal fundus images	20, 40, 60,80, 100, 120, 140, 160, 180, 200
Retina image bank database	Year	2018
	Dataset size	81.2 KB
	Total image	27313
	Retinal fundus images for identifying the Stargardt’s diseases	352
	Retinal fundus image size (KB)	30.6, 35.8, 38.5, 35.5, 30.0, 36.0, 51.7, 39.0, 51.4, 54.0
	No. of Retinal fundus images	20, 40, 60,80, 100, 120, 140, 160, 180, 200
DIARETDB0 - Standard Diabetic Retinopathy Database	Year	2007
	Dataset size	270MB
	Total image	130
	Normal image	20
	Diabetic retinopathy images	110
	Retinal fundus image size (KB)	1.52, 1.61, 1.6, 1.58, 1.56, 1.57, 1.63, 1.32, 1.68, 1.73
	No. of Retinal fundus images	12, 24, 36, 48,60, 72, 84, 96, 108, 120

4.1 Result & Discussion

The performance analysis of the proposed DNP-MDMSMSIC method and three existing methods such as [1] [2] and [29] results are discussed and analyzed. The metrics for performance analysis of proposed and existing methods are explained. All the experimentation has been carried out by the same dataset to compare the performance results. The following testing metrics are used for validating the results of the DNP-MDMSMSIC method with existing methods.


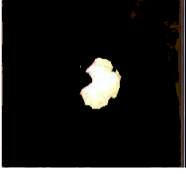


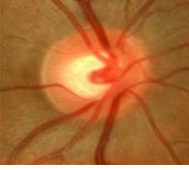

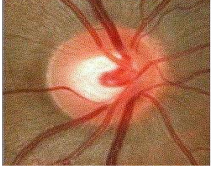

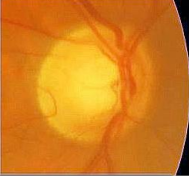
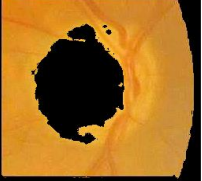
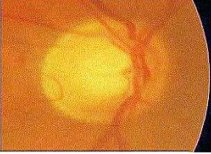
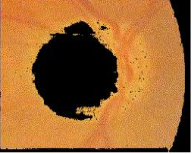
 <p>(a) Retinal fundus images</p>	 <p>(b) Accurately classified fundus image</p>
 <p>(c) Retinal fundus images</p>	 <p>(d) Misclassified retinal fundus image</p>
 <p>(e) Retinal fundus images with low PSNR</p>	 <p>(f) Misclassified retinal fundus image with low PSNR</p>
 <p>(g) Retinal fundus images with lower PSNR</p>	 <p>(h) Accurate classification retinal fundus image with lower PSNR</p>
 <p>(i) Normal fundus images with high PSNR</p>	 <p>(j) Misclassified fundus image with high PSNR</p>
 <p>(k) Normal fundus images with lower PSNR</p>	 <p>(l) Accurate classification fundus image with lower PSNR</p>

Fig. 7: (a and c) Retinal fundus images, (b) Accurately classified fundus image, (d) Misclassified retinal fundus image, (e) Retinal fundus images with high PSNR, (f) Misclassified retinal fundus image with low PSNR, (g) Retinal fundus images with lower PSNR, (h) Accurate classification retinal fundus image with lower PSNR, i) Normal fundus images with high PSNR, j) Misclassified fundus image with high PSNR, k) Normal fundus images with lower PSNR, l) Accurate classification fundus image with lower PSNR

In the proposed method, the retinal fundus images (i.e., disease images) are classified accurately shown in fig. 7 (a) and (b). The retinal fundus images (i.e., disease images) are misclassified. For example, Optic disc covered by retinal vessels tend to be misclassified. Three types of fundus images are misclassified in the proposed method and the results in the misclassifications are shown in Fig 7 (c) and (d) retinal fundus image and misclassified retinal fundus image. Fig 7 (e) and (f), normal fundus images with lower PSNR into misclassified retinal fundus image with lower PSNR. Fig 7 (i) and (j) Normal retinal fundus images with high PSNR (i.e., without disease image) and misclassified fundus image with high PSNR. The retinal fundus images with lower PSNR (i.e., without disease image) however outcomes in accurate classification are depicted in fig 7 (g) and (h). The normal fundus images with higher PSNR (i.e., without disease image) however outcomes in accurate classification are depicted in fig 7 (g) and (h).

4.2 Disease detection accuracy

D_{ACC} is defined as proportion of number of retinal fundus images are accurately detected as normal or diseased to total number of retinal fundus images. D_{ACC} is computed in percentage (%) and given below,

$$D_{ACC} = \left[\frac{AD_{RI}}{RI_m} \right] * 100 \quad (12)$$

From (12), ' D_{ACC} ' refers to disease detection accuracy, ' AD_{RI} ' denotes accurately detected disease or normal retinal images and ' RI_m ' denotes input retinal fundus images.

Table 2(a): Comparison based on disease detection accuracy using ACRIMA database

No. of Retinal fundus images	Disease detection accuracy (%)			
	DNP-MDMSMIC	OD Localization method	DCNN	SVM
20	85	80	75	70
40	88	83	78	73
60	90	87	83	76
80	92	89	86	79
100	91	88	82	76
120	95	88	83	79
140	93	89	85	81
160	92	87	84	80
180	95	89	87	84
200	94	88	86	83

Table 2(b): Comparison based on disease detection accuracy using retina image bank database

No. of Retinal fundus images	Disease detection accuracy (%)			
	DNP-MDMSMSIC	OD Localization method	DCNN	SVM
20	80	75	70	66
40	85	80	75	68
60	88	85	80	71
80	91	88	84	75
100	89	86	80	72
120	94	86	82	75
140	91	87	84	78
160	91	86	82	76
180	94	88	85	80
200	93	87	84	79

Table 2(c): Comparison based on disease detection accuracy using DIARETDB0 – Standard Diabetic Retinopathy Database

No. of Retinal fundus images	Disease detection accuracy (%)			
	DNP-MDMSMSIC	OD Localization method	DCNN	SVM
12	78	72	68	63
24	83	78	73	68
36	86	83	78	72
48	89	86	82	77
60	87	84	82	76
72	88	84	80	75
84	89	85	82	76
96	90	84	80	74
108	92	86	83	75
120	91	85	82	74

Table 2 (a), Table 2 (b), and Table 2 (c), show the results of D_{ACC} using three databases. D_{ACC} Of DNP-MDMSMSIC method is improved than the other three methods. Totally ten different results are obtained for different input retinal fundus images. In table 1 (a), the number of retinal images is represented as glaucoma disease. This is due to the application of mean shift mode seeking segmentation and the Bregman divergence function. The feature extraction images are segmented into different parts. Then the distance between two segmented regions and the image is measured to classify the disease into diverse classes with lesser error. This leads to an increase in the accuracy of disease detection in DNP-MDMSMSIC as compared to conventional methods. The disease detection accuracy of DNP-MDMSMSIC is improved by 5%, 10% and 17% as compared to [1], [2] and [29] using ACRIMA database. D_{ACC} of retina image bank database is increased by 6%, 11% and 21% as compared to [1],[2] and [29]. D_{ACC} of DIARETDB0 - Standard Diabetic Retinopathy Database is enhanced by 6%, 11% and 20% as compared to [1], [2] and [29] shown in Figures 8a, 8b, and 8c.

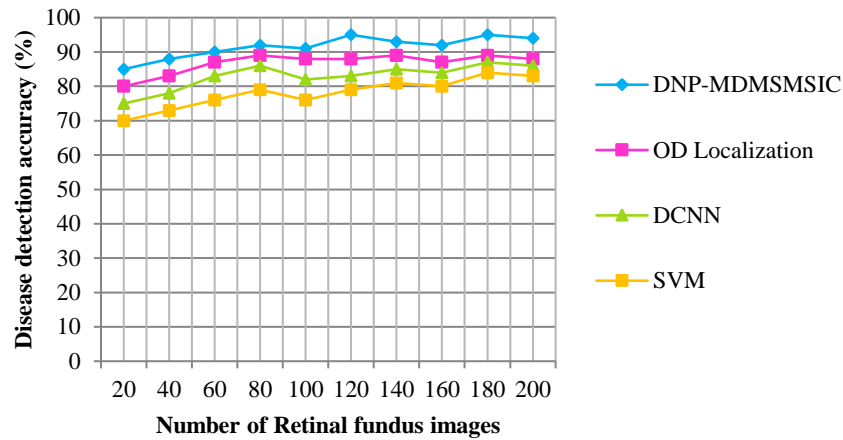


Fig. 8(a): Plot showing the results of disease detection accuracy for ACRIMA database

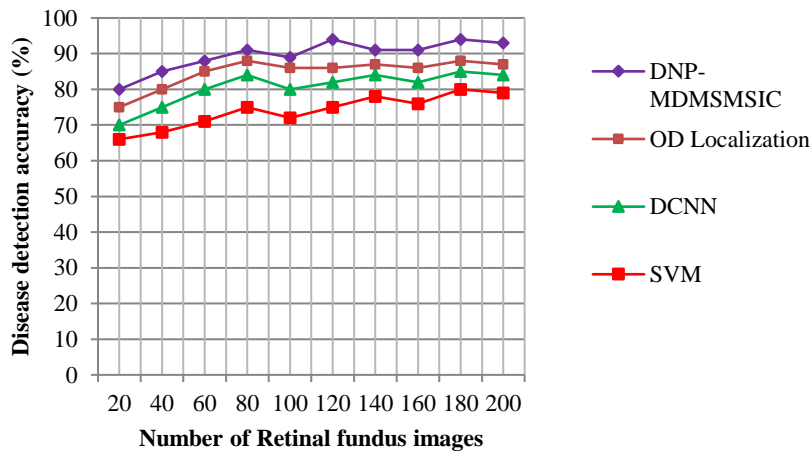


Fig. 8(b): Results of disease detection accuracy for retina image bank database

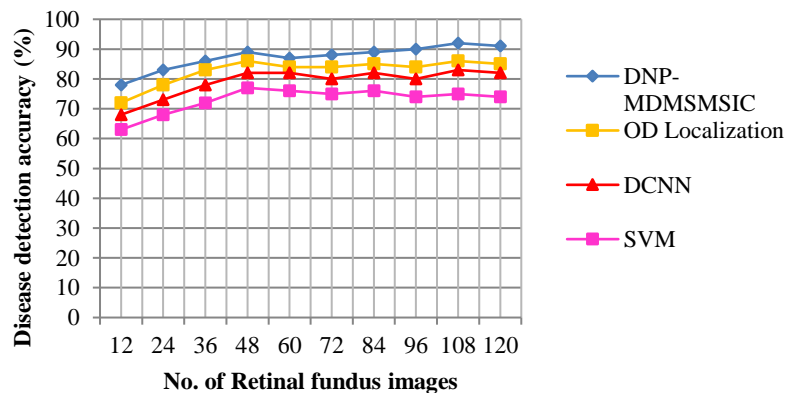


Fig. 8(c): Results of disease detection accuracy for DIARETDB0 - Standard Diabetic Retinopathy Database

Figure 8 a, 8 b, and 8 c shows the experimental results analysis of disease detection accuracy using three different methods with three datasets. The impact of disease detection accuracy along with the different number of retinal fundus images using the proposed DNP-MDMSMSIC method is evaluated with existing methods such as the OD Localization method [1], DCNN [2] and SVM [29].

4.3 Peak signal to noise ratio

‘PSNR’ is calculated as the quality measurement of the difference between the original image and the compressed image. PSNR is measured in decibel (dB). The MSE denotes the increasing squared error between the compressed and the original image. ‘PSNR’ is expressed as,

$$MSE = \frac{\sum_{m,n} [I_1(m,n) - I_2(m,n)]^2}{M*N} \quad (13)$$

$$PSNR = 10 * \log_{10} \left[\frac{R^2}{MSE} \right] \quad (14)$$

From (13), (14), ‘MSE’ refers to a mean square error. The compressed image size is denoted as ‘ $I_1(m, n)$ ’ and the original input image size is indicated as ‘ $I_2(m, n)$ ’. ‘M’ and ‘N’ denotes the number of rows and columns in the input images ‘PSNR’ denotes peak signal-to-noise ratio and ‘R’ denotes maximum possible pixel range (i.e. R=255).

Table 3(a): Comparison based on peak signal to noise ratio using ACRIMA database

Retinal fundus image sizes (KB)	Peak signal to noise ratio (dB)			
	DNP-MDMSMSIC	OD Localization	DCNN	SVM
21.3	48.13	42.11	41.28	39.05
15.4	58.58	52.57	49.04	46.54
9.13	60.9	50.86	47.07	44.43
16.5	62.11	52.57	48.13	45.21
19.7	58.59	51.23	47.3	44.61
26.3	62.11	52.57	48.13	45.85
17.9	56.09	51.23	46.55	44.61
32.2	52.57	47.3	44.05	42.25
11.7	58.59	51.23	48.13	45.85
10.2	56.09	48.13	45.21	43.52

Table 3(b): Comparison based on peak signal to noise ratio using retina image bank database

Retinal fundus image sizes (KB)	Peak signal to noise ratio (dB)			
	DNP-MDMSMSIC	OD Localization	DCNN	SVM
30.6	52.57	50.07	48.13	45.85
35.8	54.15	48.13	47.3	44.04
38.5	49.05	46.54	44.05	41.68
35.5	56.09	49.05	45.85	44.04
30.0	51.23	45.21	43.02	42.11
36.0	51.23	46.56	43.52	42.11
51.7	54.15	48.13	45.2	43.52
39.0	48.13	45.21	43.52	42.11
51.4	54.15	45.85	44.6	42.55
54.0	56.09	51.22	47.3	44.04

Table 3(c): Comparison based on peak signal to noise ratio using DIARETDB0 - Standard Diabetic Retinopathy Database

Retinal fundus image sizes (KB)	Peak signal to noise ratio (dB)			
	DNP-MDMSMSIC	OD Localization	DCNN	SVM
1.52	78.58	70.06	66.54	62.22
1.61	82.11	69.04	65.85	60.46
1.6	76.08	68.13	65.2	58.84
1.58	78.58	72.56	70.06	64.78
1.56	74.15	70.06	67.3	61.55
1.57	71.22	65.85	64.04	58.48
1.63	70.06	67.3	65.85	59.43
1.32	78.58	72.56	68.13	62.55
1.68	72.56	67.3	64.6	60.78
1.73	72.58	71.22	67.3	62.12

Table 3 (a), Table3 (b), and Table3 (c) describes SNR_p with different sizes of images from three databases. Among the four methods, the DNP-MDMSMSIC method provides higher SNR_p . In table 3 (b), the number of retinal images is indicated as Stargardt's disease.

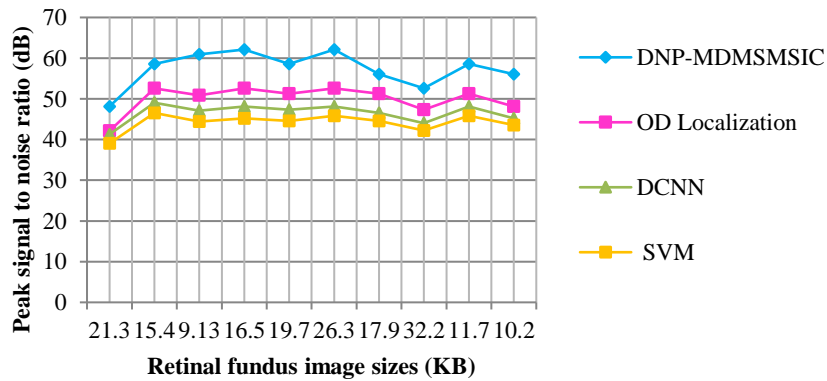


Fig. 9(a): Results of peak signal to noise ratio for ACRIMA database

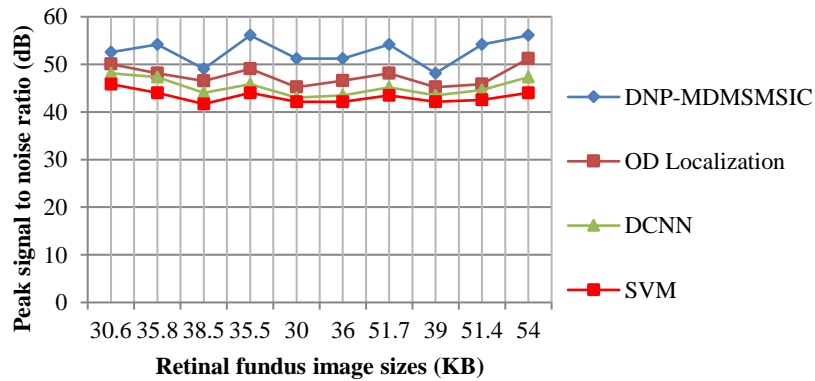


Fig. 9(b): Results of peak signal to noise ratio for retina image bank database

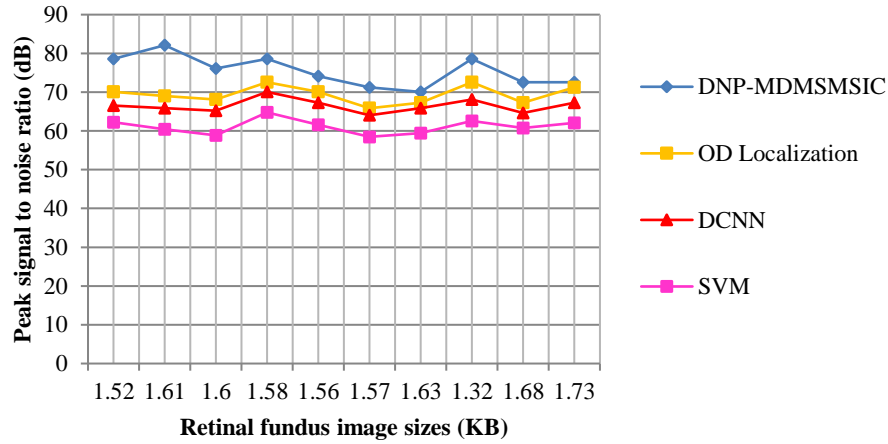


Fig. 9(c): Results of peak signal to noise ratio for DIARETDB0 - Standard Diabetic Retinopathy Database

Figure 9(a), 9(b), and 9(c) demonstrates the results analysis of peak signal-to-noise ratio using the proposed method, existing [1] [2] and [29] for three databases. The proposed DNP-MDMSMSIC method provides a greater peak signal-to-noise ratio for disease detection as compared to conventional methods. The performance of better peak signal-to-noise ratio is achieved by applying image pre-processing model called space-variant Perona–Malik diffusion. During the image pre-processing the variation between neighboring pixel, and intensity is measured to remove the noisy pixel. At this time, the image content like lines, and edges are preserved to enhance image quality. With these feature extraction images, the noise level is highly reduced and thus the performance of the peak signal to noise ratio is improved. The DNP-MDMSMSIC method increases SNR_p with ACRIMA by 15%, 23% and 30% as compared to [1], [2] and [29]. SNR_p For retina image bank database is improved by 11%, 16% and 22% as compared to [1], [2] and [29]. SNR_p for DIARETDB0 - Standard Diabetic Retinopathy Database is enhanced by 8%, 13% and 23% as compared to [1], [2] and [29] shown in figures 9a, 9b, and 9c.

4.4 Disease Detection Time

Disease detection time (t_{GDD}) is calculated as amount of time consumed to detect disease or normal image. t_{GDD} Is determined in milliseconds (ms). The mathematical expression to compute the t_{GDD} is provided as follows,

$$t_{GDD} = RI_m * Time (d_{SI}) \quad (15)$$

From (15), ' d_{SI} ' is the single image detection. The minimum value of time indicates a better performance of disease detection. Table 4 (a), Table4 (b), and Table4 (c) shows the results of t_{GDD} with the number of retinal fundus images. t_{GDD} Using the DNP-MDMSMSIC method is decreased than the state-of-the-art methods. In table 4 (c), the number of retinal images is indicated as glaucoma and Stargardt's disease.

Table 4(a): Comparison based on disease detection time using ACRIMA database

No. of Retinal fundus images	Disease detection time (ms)			
	DNP-MDMSMSIC	OD Localization	DCNN	SVM
20	15	20	24	27
40	17	22	26	29
60	21	25	29	32
80	23	28	32	34
100	27	32	36	39
120	31	35	39	41
140	33	37	42	45
160	38	42	45	48
180	40	44	49	52
200	42	47	51	54

Table 4(b): Comparison based on disease detection time using retina image bank database

No. of Retinal fundus images	Disease detection time (ms)			
	DNP-MDMSMSIC	OD Localization	DCNN	SVM
20	18	23	27	30
40	19	25	29	32
60	22	26	31	34
80	25	28	32	36
100	26	30	34	37
120	31	35	38	41
140	35	38	42	45
160	39	42	46	49
180	40	45	50	52
200	43	47	52	55

Table 4(c): Comparison based on disease detection time using DIARETDB0 - Standard Diabetic Retinopathy Database

No. of Retinal fundus images	Disease detection time (ms)			
	DNP-MDMSMSIC	OD Localization	DCNN	SVM
12	13	20	25	28
24	16	22	27	30
36	18	24	29	32
48	21	26	30	34
60	23	28	32	36
72	27	30	36	39
84	31	33	40	43
96	33	37	42	45
108	36	40	48	50
120	38	45	50	53

The above table 4(a), (b), (c) shows the comparison results of ' t_{GDD} ' with respect to the different number of retinal fundus images.

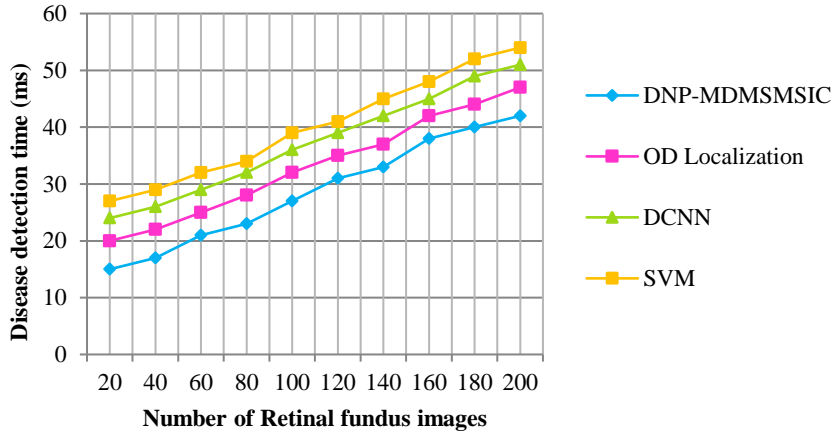


Fig. 10(a): Results of disease detection time for ACRIMA database

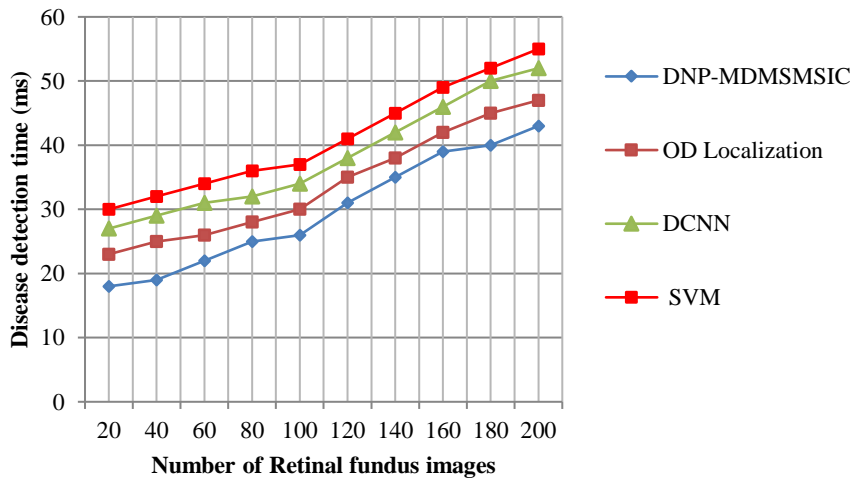


Fig. 10(b): Results of disease detection time for retina image bank database

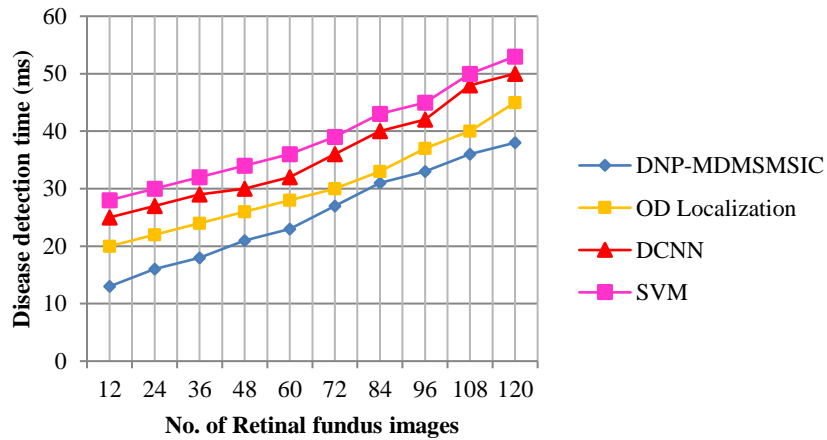


Fig. 10(c): Results of disease detection time for DIARETDB0 - Standard Diabetic Retinopathy Database

Figure 10 a, 10 b, and 10 c depicts the results analysis of ‘ t_{GDD} ’ with respect to diverse number of retinal fundus images using proposed and existing [1] [2] and [29]. In the above graph, x-axis shows the number of retinal images and the corresponding time to detect the disease is given in the y-axis. As presented in the above graphical plot, the proposed DNP-MDMSMSIC method gives lower amount of time consumption for disease detection than the other methods. The minimal amount of time complexity is attained with the process of pre-processing and feature extraction. At first, space-variant Perona–Malik diffusion is employed to de-noise the input images. This leads to enhance the contrast for further analysis. Then the features for disease detection such as color, texture and intensity are automatically extracted using the deep learning model of the DNP-MDMSMSIC method. This considerably lessens the overall time consumption for early disease detection. ‘ t_{GDD} ’ of DNP-MDMSMSIC method using ACRIMA database is reduced by 15%, 25% and 30% as compared to [1],[2] and [29]. t_{GDD} of retina image bank database is minimized by 13%, 23% and 29% as compared to [1], [2] and [29]. t_{GDD} of DIARETDB0 - Standard Diabetic Retinopathy Database is reduced by 18%, 30% and 36% as compared to [1], [2] and [29] shown in figures10a, 10b, and 10c.

4.5 Error Rate

Error rate (R_E) is determined as ratio of number of retinal fundus images are wrongly detected from input images. R_E is expressed as follows.

$$R_E = \left(\frac{WD_{RI}}{R_{Im}} \right) * 100 \quad (16)$$

From (16), ‘ WD_{RI} ’ denotes wrongly detected retinal images. R_E is measured in percentage (%). Table 5 (a), Table 5 (b), and Table 5 (c) illustrates R_E with the number of retinal fundus images using two diverse datasets. In table 5 (a), the number of retinal images is referred to as glaucoma disease. By analyzing the above table, the amount of retinal fundus images incorrectly detected is reduced in DNP-MDMSMSIC.

Table 5(a): Comparison based on error rate using ACRIMA database

No. of Retinal fundus images	Error rate (%)			
	DNP-MDMSMSIC	OD Localization	DCNN	SVM
20	15	20	25	30
40	12	17	22	27
60	10	13	17	24
80	8	11	14	21
100	9	12	18	24
120	5	12	17	21
140	7	11	15	19
160	8	13	16	20
180	5	11	13	16
200	6	12	14	17

Table 5(b): Comparison based on error rate using retina image bank database

No. of Retinal fundus images	Error rate (%)			
	DNP-MDMSMSIC	OD Localization	DCNN	SVM
20	20	25	30	34
40	15	20	25	32
60	12	15	20	29
80	9	12	16	25
100	11	14	20	28
120	6	14	18	25
140	9	13	16	22
160	9	14	18	24
180	6	12	15	20
200	7	13	16	21

Table 5 (c): Comparison based on error rate using DIARETDB0 - Standard Diabetic Retinopathy Database

No. of Retinal fundus images	Error rate (%)			
	DNP-MDMSMSIC	OD Localization	DCNN	SVM
12	22	28	32	37
24	17	22	27	32
36	14	17	22	28
48	11	14	18	23
60	13	16	18	24
72	12	16	20	25
84	11	15	18	24
96	10	16	20	26
108	8	14	17	25
120	9	15	18	26

Table 5(a), (b), and (c) illustrate the performance comparison of R_E based on the number of retinal fundus images using two diverse datasets. In experiments, the results of R_E using the DNP-MDMSMSIC method is evaluated with the existing OD Localization method [1], DCNN [2], and SVM [29].

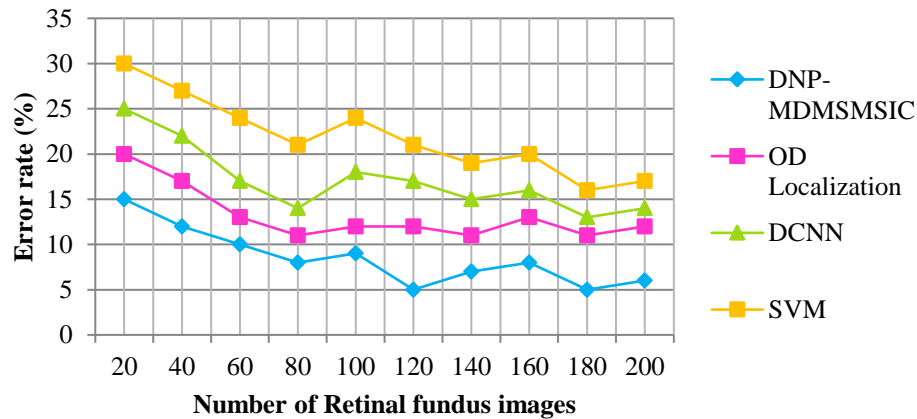


Fig.11(a): Experimental results of error rate for ACRIMA database

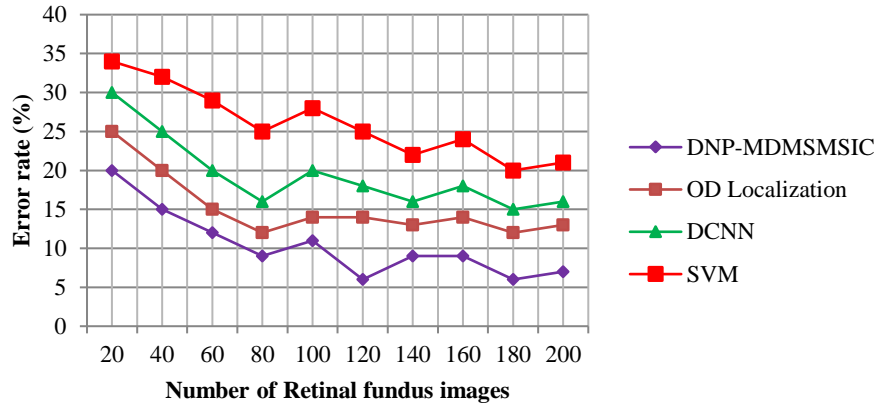


Fig.11(b): Experimental results of error rate for retina image bank database

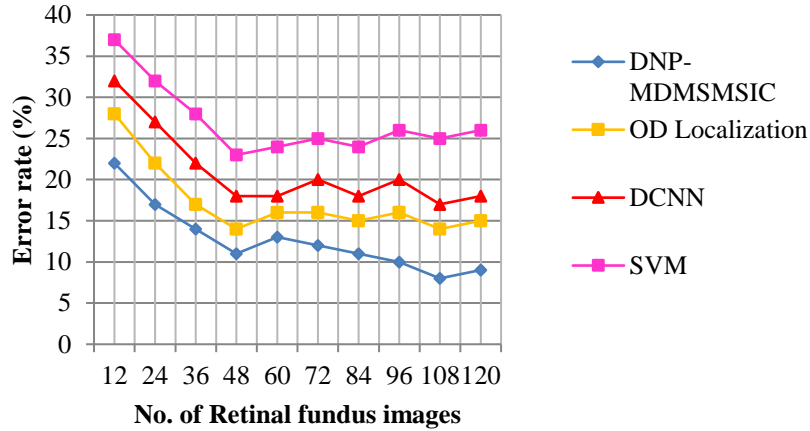


Fig. 11(c): Experimental results of error rate for DIARETDB0 - Standard Diabetic Retinopathy Database

Figure 11 a, 11 b, and 11 c demonstrates the results analysis of R_E depends on the diverse number of retinal fundus images from different datasets. As shown in the graphical plot, the proposed DNP-MDMSMSIC method gives a minimal error during disease detection when compared to state-of-the-art methods. A lower amount of error is achieved with the design of accurate segmentation and classification process in the DNP-MDMSMSIC method. A similar set of pixels in the retinal fundus images are divided into number of segments by using the mean shift procedure. Then the partitioned images are categorized by measuring the distance between them using the Bergman function. In addition, the error in the output layer is measured to give minimal misclassification results. This leads to an efficient decrease the disease detection error. DNP-MDMSMSIC method using ACRIMA database reduces R_E by 37%, 51% and 62% as compared to [1], [2] and [29]. R_E using retina image bank database is decreased by 33%, 48% and 61% as compared to [1], [2] and [29]. R_E using DIARETDB0 - Standard Diabetic Retinopathy Database is reduced by 27%, 40% and 54% as compared to [1], [2] and [29] shown in figures 11a, 11b, and 11c.

4.6 Performance measure of SSIM

The structural similarity index ‘SSIM’ is computed based on the mean values, standard deviation, and cross variance and is mathematically calculated as given below.

$$SSIM(i, j) = \frac{(2\mu_i\mu_j + C_1)(2\sigma_{ij} + C_2)}{(\mu^2_i + \mu^2_j + C_1)(\sigma^2_i + \sigma^2_j + C_2)} \quad (17)$$

In the above equation (17), ‘SSIM’ is indicated as the structural similarity index, and the mean values are represented as ‘ $\mu_i\mu_j, \mu^2_i, \mu^2_j$ ’, the standard deviation is indicated as ‘ σ^2_i, σ^2_j ’ and the cross variance is represented as ‘ σ_{ij} ’ for brain tumor images ‘ i, j ’ respectively.

Table 6(a): Comparison based on SSIM using ACRIMA database

Retinal fundus image sizes (KB)	SSIM			
	DNP-MDMSMSIC	OD Localization	DCNN	SVM
21.3	0.915	0.785	0.745	0.685
15.4	0.885	0.775	0.705	0.655
9.13	0.825	0.735	0.675	0.625
16.5	0.835	0.715	0.655	0.605
19.7	0.855	0.775	0.725	0.645
26.3	0.875	0.795	0.745	0.675
17.9	0.895	0.835	0.765	0.695
32.2	0.865	0.815	0.755	0.675
11.7	0.9	0.84	0.775	0.685
10.2	0.915	0.865	0.8	0.695

Table 6(b): Comparison based on SSIM using retina image bank database

Retinal fundus image sizes (KB)	SSIM			
	DNP-MDMSMSIC	OD Localization	DCNN	SVM
30.6	0.945	0.805	0.765	0.695
35.8	0.915	0.795	0.725	0.675
38.5	0.885	0.755	0.695	0.645
35.5	0.875	0.735	0.675	0.625
30.0	0.905	0.795	0.745	0.685
36.0	0.915	0.805	0.765	0.695
51.7	0.935	0.855	0.785	0.705
39.0	0.905	0.835	0.775	0.725
51.4	0.94	0.86	0.795	0.745
54.0	0.945	0.885	0.82	0.765

Table 6(c): Comparison based on SSIM using DIARETDB0 - Standard Diabetic Retinopathy Database

Retinal fundus image sizes (KB)	SSIM			
	DNP-MDMSMSIC	OD Localization	DCNN	SVM
1.52	0.965	0.825	0.785	0.715
1.61	0.935	0.815	0.745	0.675
1.6	0.905	0.775	0.715	0.655
1.58	0.885	0.755	0.695	0.625
1.56	0.915	0.815	0.765	0.685
1.57	0.925	0.825	0.785	0.695
1.63	0.945	0.875	0.805	0.725
1.32	0.925	0.855	0.795	0.735
1.68	0.96	0.88	0.815	0.755
1.73	0.965	0.895	0.84	0.775

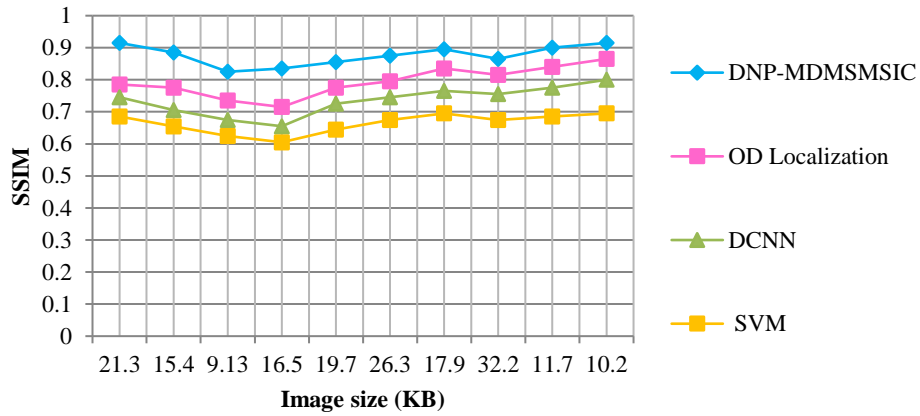


Fig. 12(a): Results of SSIM for ACRIMA database

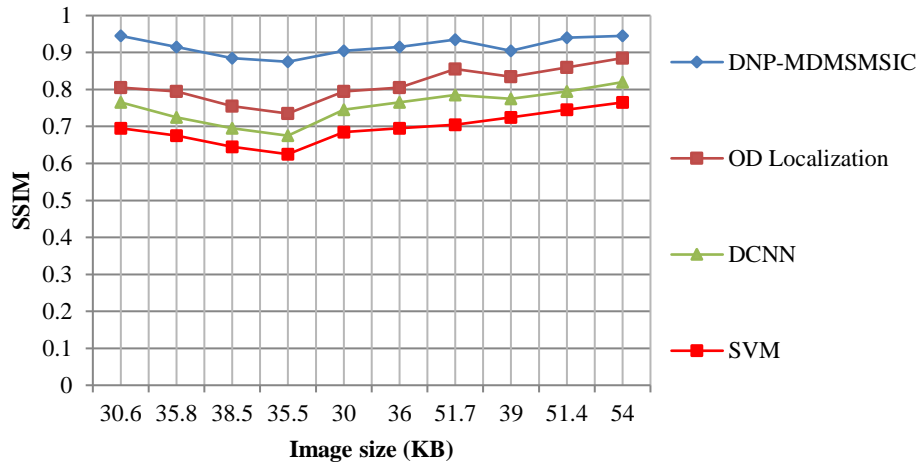


Fig. 12(b): Results of SSIM for retina image bank database

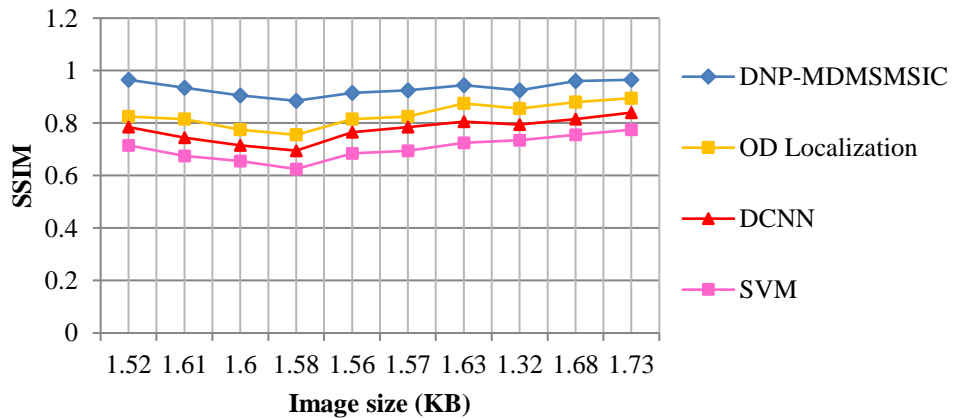


Fig. 12(c): Results of SSIM for DIARETDB0 - Standard Diabetic Retinopathy Database

Figure 12 a, 12 b, and 12 c shows the experimental results analysis of SSIM with respect to 10 dissimilar images of different sizes. This is owing to the application of mean shift mode seeking segmentation and Bregman divergence function. The DNP-MDMSMSIC method increases SSIM with ACRIMA by 11%, 20% and 32% as compared to [1], [2] and [29]. SSIM for retina image bank database is improved by 13%, 22% and 32% as compared to [1], [2] and [29]. SSIM for DIARETDB0 - Standard Diabetic Retinopathy Database is enhanced by 12%, 21% and 33% as compared to [1], [2] and [29].

5.0 CONCLUSION

A DNP-MDMSMSIC method is designed to detect Glaucoma and Stargardt's disease, at early stage Space-variant Perona–Malik diffusive image pre-processing is performed to de-noise the input image to improve image quality. The color, texture, and intensity features are extracted with higher accuracy for disease detection. By considering these extracted features, the feature extraction images are segmented. Further processing of the images in the designed algorithm, segments the pixels in image space by identifying the local maxima modes of each pixel. These segmented images are classified by determining the distance between two segmented regions. Then, retinal fundus images are classified. This enhances the disease detection using DNP-MDMSMSIC. The result of the DNP-MDMSMSIC method improves disease detection accuracy with lesser time and error as compared to OD localization method DCNN. The proposed DNP-MDMSMSIC method is further implemented to enhance accuracy and reduce time consumption by using novel deep learning techniques.

6.0 FINANCIAL DISCLOSURE

We have not received any fund from the institutions.

REFERENCES

- [1] W. Luangruangrong and K. Chinnasarn, "Optic Disc Localization in Complicated Environment of Retinal Image Using Circular-Like Estimation", *Arabian Journal for Science and Engineering*, Vol. 44, 2019, pp. 4009–4026, doi: 10.1007/s13369-019-03756-3.
- [2] R. Murugan, P. Roy and U. Singh, "An abnormality detection of retinal fundus images by deep convolutional neural networks. *Multimedia Tools and Applications*", Vol. 79, 2020, pp. 1-19 (2020), doi: 10.1007/s11042-020-09217-6.
- [3] Z. U. Rehman, S. S. Naqvi, T. M. Khan, M. Arsalan, M. A. Khan and M. A. Khalil, "Multi-parametric Optic Disc Segmentation Using Superpixel Based Feature Classification. *Expert Systems with Applications*", Vol. 120, 2019, pp. 461-473, doi: 10.1016/j.eswa.2018.12.008.
- [4] S. Maheshwari, V. Kanhangad, R. B. Pachori, S. V. Bhandary and U. R. Acharya, "Automated glaucoma diagnosis using bit-plane slicing and local binary pattern techniques", *Computers in Biology and Medicine*, Vol. 105, 2019, pp. 72-80, doi: 10.1016/j.compbiomed.2018.11.028.
- [5] M. Juneja, N. Thakur, S. Thakur, A. Uniyal, A. Wani and P. Jindal, "GC-NET for classification of glaucoma in the retinal fundus image", *Machine Vision and Applications*, Vol. 31, 2020, pp 1-18, doi:10.1007/s00138-020-01091-4
- [6] C. Bowd, A. Belghith, J. A. Proudfoot, L. M. Zangwill, M. Christopher, M. H. Goldbaum, H. Hou, R. C. Pentead, S. Moghimi and R. N. Weinreb, "Gradient-Boosting Classifiers Combining Vessel Density and Tissue Thickness Measurements for Classifying Early to Moderate Glaucoma", *American Journal of Ophthalmology*, Vol. 217, 2020, pp.131-139, doi:10.1016/j.ajo.2020.03.024.
- [7] D. A. Dharmawan, B. P. Ng and S. Rahardja "A new optic disc segmentation method using a modified Dolph-Chebyshev matched filter", *Biomedical Signal Processing and Control*, Vol. 59, 2020, pp.1-10, doi:10.1016/j.bspc.2020.101932.

- [8] J. Pruthi, K. Khanna and S. Arora “Optic Cup segmentation from retinal fundus images using Glowworm Swarm Optimization for glaucoma detection,” *Biomedical Signal Processing and Control*, Vol. 60, 2020, pp.1-12, doi:10.1016/j.bspc.2020.102004.
- [9] A.Mvoulana, R. Kachouri and M. Akil, “Fully automated method for glaucoma screening using robust optic nerve head detection and unsupervised segmentation based cup-to-disc ratio computation in retinal fundus images”, *Computerized Medical Imaging and Graphics*, Vol. 77, 2019, pp.1-19, doi:10.1016/j.compmedimag.2019.101643.
- [10] J. Martins, J. S. Cardoso and F. Soares, “Offline computer-aided diagnosis for Glaucoma detection using fundus images targeted at mobile devices”, *Computer Methods and Programs in Biomedicine*, Vol. 192, 2020, pp.1-14, doi: 10.1016/j.cmpb.2020.105341.
- [11] L. Abdel-Hamid, “Glaucoma Detection from Retinal Images Using Statistical and Textural Wavelet Features”, *Journal of Digital Imaging*, Vol.33, 2020, pp.151–158, DOI: 10.1007/s10278-019-00189-0.
- [12] D. S. David and A. Jayachandran, “A new expert system based on hybrid colour and structure descriptor and machine learning algorithms for early glaucoma diagnosis”, *Multimedia Tools and Applications*, Vol. 79, 2020, pp. 5213–5224, doi:10.1007/s11042-018-6265-1.
- [13] U. Raghavendra, A. Gudigar, S. V. Bhandary, T. N. Rao, E. J. Ciaccio and U. R. Acharya, “A Two Layer Sparse Autoencoder for Glaucoma Identification with Fundus Images”, *Image & Signal Processing*, Vol.43, 2019, pp. 1-9, doi: 10.1007/s10916-019-1427-x.
- [14] M. N. Bajwa, M. I. Malik, S. A. Siddiqui, A. Dengel, F. Shafait, W. Neumeier and S. Ahmed, “Two-stage framework for optic disc localization and glaucoma classification in retinal fundus images using deep learning” *BMC Medical Informatics and Decision Making*, Vol. 19, 2019, pp. 1-16, doi:10.1186/s12911-019-0842-8.
- [15] N. Thakur and J. Mamta, “Survey on segmentation and classification approaches of optic cup and optic disc for diagnosis of glaucoma”, *Biomedical Signal Processing and Control*, Vol 42, 2018, pp. 162-189, doi:10.1016/j.bspc.2018.01.014.
- [16] R. G. Ramani and J. J. Shanthamalar. “Improved image processing techniques for optic disc segmentation in retinal fundus images”, *Biomedical Signal Processing and Control*, Vol. 58, 2020, pp. 1-18, doi:10.1016/j.bspc.2019.101832.
- [17] T. S.Rama Perumal and Dhanasekaran,R. “Early diagnosis of Glaucoma in retinal images using multi structure descriptor and hybrid neural network classifiers”, *Multimedia Tools and Applications*, Vol. 79, 2020, pp. 16915–16925, doi:10.1007/s11042-019-7428-4.
- [18] M. d. L. Claro, R. Veras, A. Santana, F. H. D. Araújo, R. Silva, J. Almeida and D. Leite, “An hybrid feature space from texture information and transfer learning for glaucoma classification”, *Journal of Visual Communication and Image Representation*, Vol. 64, 2019, pp. 1-12, doi:10.1016/j.jvcir.2019.102597.
- [19] F. Li, L. Yan, Y. Wang, J. Shi, H. Chen, X. Zhang, M. Jiang, Z. Wu and K. Zhou. “Deep learning-based automated detection of glaucomatous optic neuropathy on color fundus photographs”, *Graefe's Archive for Clinical and Experimental Ophthalmology*, Vol.258, 2020, pp. 851-867, doi: 10.1007/s00417-020-04609-8.
- [20] F. Ajesh, R. Ravi and G. Rajakumar, “Early diagnosis of glaucoma using multi-feature analysis and DBN based classification”, *Journal of Ambient Intelligence and Humanized Computing*, Vol. 12, 2020, pp.4027–4036, doi:10.1007/s12652-020-01771-z.
- [21] B. Antal, A. Hajdu, Z. Maros-Szabo, Z. Torok, A. Csutak and T. Peto. “A two-phase decision support framework for the automatic screening of digital fundus images”, *Journal of Computational Science*, Vol. 3, 2012, pp. 262-268, doi:10.1016/j.jocs.2012.01.001.

- [22] J. H. Tan, U. R. Acharya, S. V. Bhandary, K. C. Chua and S. Sivaprasad, “Segmentation of optic disc, fovea and retinal vasculature using a single convolutional neural network”, *Journal of Computational Science*, Vol. 20, 2017, pp.70-79, doi:10.1016/j.jocs.2017.02.006.
- [23] J. Amin, M. Sharif, M. Yasmin, H. Ali and S. L. Fernandes, “A Method for the Detection and Classification of Diabetic Retinopathy Using Structural Predictors of Bright Lesions”, *Journal of Computational Science*, Vol. 19, 2017, pp. 153-164, doi:10.1016/j.jocs.2017.01.002.
- [24] P. Tanna, R. W Strauss, K. Fujinami, and M. Michaelides, “Stargardt disease: clinical features, molecular genetics, animal models and therapeutic options”, *The British Journal of Ophthalmology*, Vol. 101, 2017, pp. 25-30 doi: 10.1136/bjophthalmol-2016-308823.
- [25] M. Juneja, S. Thakur, A. Uniyal, A. Wani, N. Thakura and P. Jindal, “Deep learning-based classification network for glaucoma in retinal images”, Elsevier, *Computers and Electrical Engineering*, Vol.101, 2022, pp. 04-21, doi:10.1016/j.compeleceng.2022.108009.
- [26] H. N.Veena, A. Muruganandham and T. S. Kumaran, “A novel optic disc and optic cup segmentation technique to diagnose glaucoma using deep learning convolutional neural network over retinal fundus images”, Elsevier, *Journal of King Saud University - Computer and Information Sciences*, Vol. 34, Issue 8, 2022, pp. 6187-6198, doi:10.1016/j.jksuci.2021.02.003.
- [27] M. Sun, K. Li, X. Qi, H. D. and G. Zhang “Contextual information enhanced convolutional neural networks for retinal vessel segmentation in color fundus images”, *Journal of Visual Communication and Image Representation*, Vol.77, 2021, pp.1-12, doi:10.1016/j.jvcir.2021.103134.
- [28] M. Rezaei, F. Soleymani, B. Bischl and S. Azizi “Deep Bregman Divergence for Contrastive Learning of Visual Representations”, *arXiv Computer Science*, Vol.2, 2021, pp.1-11, doi:10.48550/arXiv.2109.07455
- [29] Y. Katada, N. Ozawa, K. Masayoshi, Y. Ofuji, K. Tsubota and T. Kurihara, “Automatic screening for diabetic retinopathy in interracial fundus images using artificial intelligence”, *Intelligence-Based Medicine*, vol. 3, 2020, pp. 1-8, doi:10.1016/j.ibmed.2020.100024.
- [30] ACRIMA database, https://figshare.com/articles/CNNs_for_Automatic_Glaucoma_Assessment_using_Fundus_Images_An_Extensive_Validation/7613135, 2019
- [31] Retina image bank database, <https://imagebank.asrs.org/file/28619/stargardt-disease>, 2018
- [32] DIARETDB0 – Standard Diabetic Retinopathy Database, <https://www.it.lut.fi/project/imageret/diaretdb0/>, 2007